Synthesis and NMR study of trimethylphosphine gold(I)-appended calix[8]arenes as precursors of gold nanoparticles

Marie Clément, Ibrahim Abdellah, Priyanka Ray, Cyril Martini, Yannick Coppel, Hynd Remita, Isabelle Lampre, Vincent Huc

ARTICLE

Synthesis and NMR study of Trimethylphosphine Gold(I)-appended Calix[8]arenes as precursors of Gold nanoparticles

Marie Clément,[a,b] Ibrahim Abdellah,*[a] Priyanka Ray, Cyril Martini*,[a,c] Yannick Coppel,*[d]] Hynd Remita,[b] Isabelle Lampre,*[b] and Vincent Huc*[a]

Received 00th January 20xx,
Accepted 00th January 20xx

DOI: 10.1039/x0xx00000x

In this paper, the synthesis of gold(I)-calix[8]arene complexes from benzyloxycalix[8]arene used as a starting material is reported. 8 or 16 trimethylphosphine-gold(I) are grafted to the calix[8] arene via a C_4 alkane chain linker and a thiolate group. The formed gold(I)-complexes are characterised by NMR spectroscopy. We also show that these complexes can act as both source of metal and stabilizing agent for the formation a gold nanoparticles as the radiolytic reduction of these complexes produces small monodisperse nanoparticles.

Introduction

Over the last few decades, gold became a central topic in organometallic chemistry. Indeed, gold's very strong relativistic effect makes it a unique element in the d block of periodic table.[1] Regarding organometallic chemistry, gold complexes have found numerous applications in organic synthesis transformations as both homogenous and heterogeneous catalysts.[2] Since the pioneering work of Hayashi using a chiral ferrocenylphosphine gold complex as catalyst for both C-C and C-O bonds formation,[3] organometallic gold complexes have been used for the activation of alkenes and alkynes, facilitating the attack of nucleophiles thanks to the strong Lewis acidity of gold.[4] Very recently other applications such as C-H,[5] C-X [6] and C-C [7] activations with gold have been developed. Since the pioneering work of Haruta in 1987,[8] catalysis by gold has attracted increasing attention. Gold nanoparticles (Au NPs) have demonstrated high activity in catalytic oxidations[9] or reduction[10] reactions, and their use in surface chemistry[11] heterogeneous catalysis[12] and nanochemistry[13] have also been explored. Size effects are crucial in catalysis by gold. The synthesis methods play an important role to control the size, the shape and subsequently the properties of the Au NPs, as well as their applications. Since the initial works of Türkevich, Brust and Schmidt,[14] considerable research efforts have been devoted towards the controlled synthesis of Au clusters and NPs. Among the numerous parameters involved for synthesis in solution, the stabilizing agent is a major one, and lately, macrocycles, such as calixarenes, have appeared as good candidates.[15]

In this context, we recently synthesized mono and bi-metallic gold (Au) - silver (Ag) NPs by radiolytic reduction of metallic salts in the presence of thiol-functionalised calix[8]arenes. It was shown that calix[8]arenes were able to stabilize small and homogeneous in size spherical metal NPs, for an adequate metal to calix[8]arene ratio.[16] In this paper, we present a new approach in which the calixarene plays the role of both a stabilising agent and a source of metal. This approach follows the recently developed strategy of using benzyloxycalix[8]arenes[17] as a platform to support N-heterocyclic carbene palladium complexes[18] or to immobilize Cobalt-salen complexes[19] for catalysis. Here, we describe the synthesis and characterisations of new calix[8]arene-supported gold complexes (Figure 1), 8 or 16 $Me_3PAu(I)$ units being bonded to each phenol site via a C_4 alkane chain linker and a thiolate group.[20] Then, we show that the reduction of these calix[8]arene-supported gold complexes by radiolysis in ethanolic solution leads to the formation of small calix[8]arene-stabilised Au NPs.

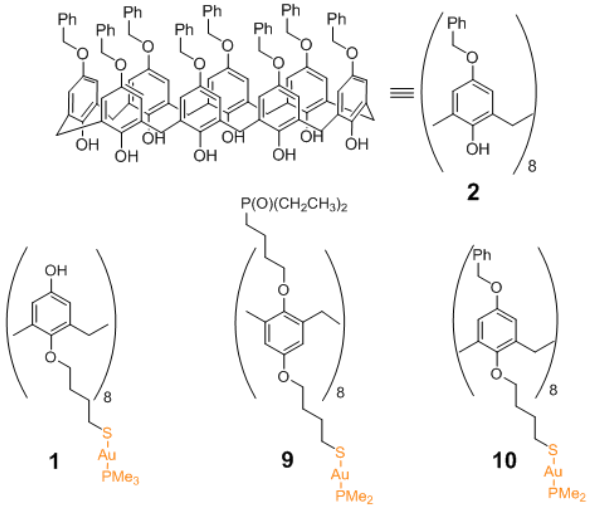

Figure 1. Molecular structures of the initial benzyloxycalix[8]are (**Top,** compound **2**). gold(I)-appended calix[8]arenes (**Down,** complexes **1**, **9** and **10**)

[a] *Institut de Chimie Moléculaire et des Matériaux d'Orsay, Univ Paris-Sud UMR 8182 CNRS, Université Paris-Saclay, 91405 Orsay cedex, France. E-mail: ibrahim_abdellah@hotmail.com ; vincent.huc@univ-psud.fr.*
[b] *Laboratoire de Chimie Physique, Univ Paris-Sud UMR 8000 CNRS, Université Paris-Saclay, 91405 Orsay cedex, France. E-mail:isabelle.lampre@u-psud.fr*
[c] *NOVECAL, 86 rue de Paris, 91400 Orsay, France. E-mail: cyril.martini@novecal.fr.*
[d] *LCC-CNRS, Université de Toulouse, 205 route de Narbonne, BP 44099, 31077 Toulouse Cedex 4, France. E-mail: yannick.coppel@lcc-toulouse.fr*

† Footnotes relating to the title and/or authors should appear here.
Electronic Supplementary Information (ESI) available: [details of any supplementary information available should be included here]. See DOI: 10.1039/x0xx00000x

Results and discussion

p-octa(hydroxyl)-octa[(mercaptobutoxy)-gold(I)trimethylphosphine]calix[8]arene

Synthesis. The synthesis of *p*-octa(hydroxyl)-octa[(mercaptobutoxy)-gold(I)trimethylphosphine]calix[8]arene **1** was realized in five steps from the benzyloxycalix[8]arene **2** (Scheme 1).[21] An excellent yield (93%) was obtained for compound **3** after chloroalkylation of the phenolic position of benzyloxycalix[8]arene **2** with 1-bromo-4-chlorobutane using NaH as a base. The benzyl group of compound **3** was then removed using $Pd(OH)_2$ in the presence of cyclohexene, providing a 98% yield of compound **4**. Nucleophilic attack at the terminal, chloride-bound carbon atoms of **4** by potassium thioacetate in DMSO afforded compound **5** in 78% yield. The synthesis of the thiol compound **6** was then achieved by hydrolysis of compound **5** with sodium methanolate (prepared in situ from methanol and sodium in THF) and subsequent addition of a solution of HCl (1 M) followed by n-Bu_3P (n-tributylphosphine), and gave a 91% yield of compound **6**.[16] The Au^IPMe_3-appended calix[8]arene **1** was then prepared from **6** and commercially-available Me_3PAuCl by simple substitution of chloride by the thiolate generated *in situ* by deprotonation of the thiol group by Et_3N. The complex **1** precipitated from the solution as a white solid, recovered after filtration and washing by THF and EtOH in 52% yield. This complex was found to be soluble only in DMF and DMSO.

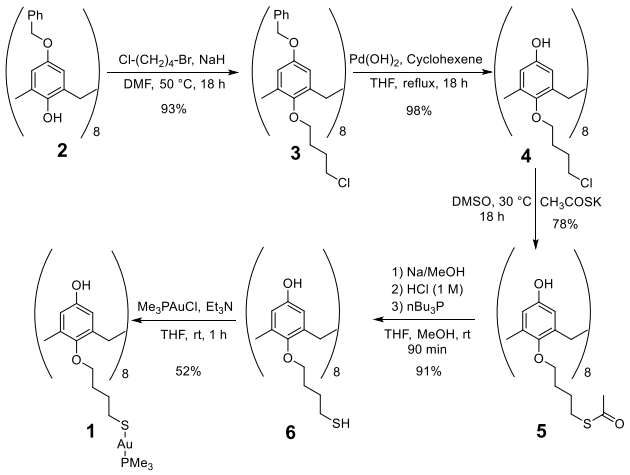

Scheme 1. Multi-steps synthesis of complex **1**.

Chemical characterisations. Complex **1** and its precursor **6** were analysed by infrared spectroscopy (KBr pellet), as shown in Figure 2. The characteristic bands of compound **6** were still observed in complex **1** apart from the S-H stretching band at 2561 cm^{-1}. This confirms the successful deprotonation of the thiol group, and is a strong indication towards the formation of the expected gold complex.

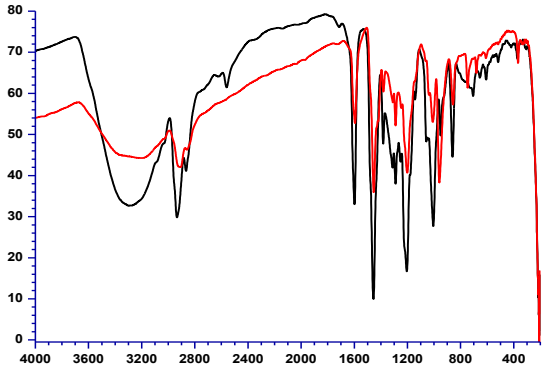

Figure 2. IR spectra of compounds **6** (black) and **1** (red).

To control the formation of complex **1**, elemental analysis (C, H and S) and X-ray photoelectron spectroscopy (XPS) were performed to get semi-quantitative analyses of complex **1** in the powder form (Table 1). The results are close to the values calculated from the overall formula ($C_{112}H_{176}Au_8O_{16}P_8S_8$).

Experiment	Elements	Theoretical (%)	Experimental (%)
Elemental analysis	C	34,86	35.4
	H	4.60	4.39
	S	6.65	6.87
XPS	C_{1s}	73.7	72.7
	O_{1s}	10.5	12.6
	Au_{4f}	5.3	5.5
	P_{2p}	5.3	3.3

Table 1. Elemental and X-ray photoelectron spectroscopy analysis of complex **1**.

NMR structural characterisations. NMR spectroscopy carried out in DMSO-d_6 at room temperature also indicates the formation of calixarene/ Me_3PAu adduct. In the ^1H NMR spectrum (Figure 3), the width of all signals of complex **1** increased compared to those of compound **6**, evidencing the reduced mobility of complex **1** due to the steric hindrance of the eight Me_3PAu groups and/or intramolecular aurophilic interactions between the gold centres. Coordination of gold to the calix[8]arene is also shown by the 0.44 ppm shift of the signal corresponding to the protons α to the sulphur atom: for compound **6** this signal peaks at 2.43 ppm, while for complex **1** the corresponding signal appears at higher frequency, 2.87 ppm (Figure 3). The ^{31}P NMR spectrum of complex **1** (Figure 4) presents a strong signal at –1.0 ppm and very weak one at 8.9 ppm compared to the signal of Me_3PAuCl (–8.1 ppm).

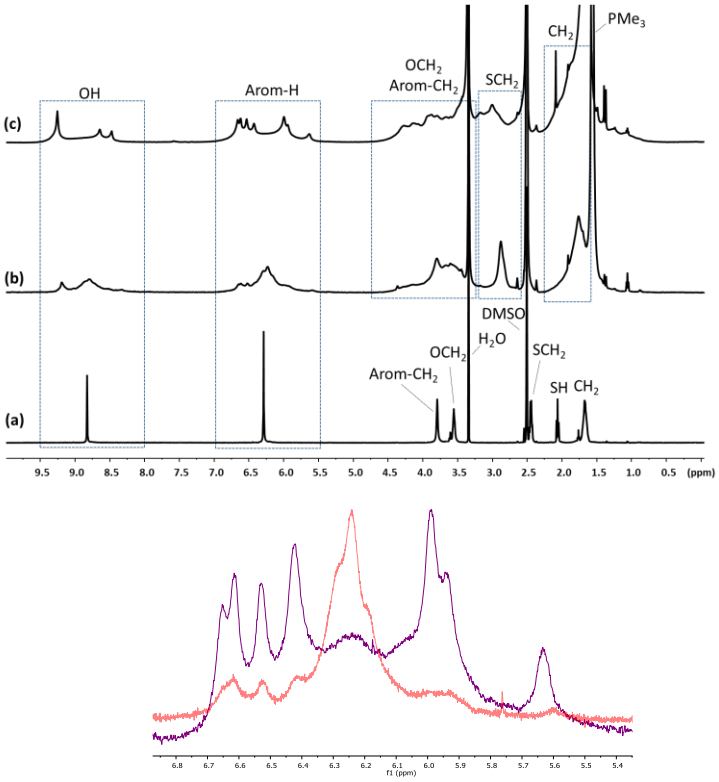

Figure 3. Top. ^{1}H NMR spectra in DMSO-d_6 at 298K of (a) compound **6**, (b) complex **1**, and (c) complex **1'** **Bottom.** Signals of the aromatic protons in complex **1** (red) and complex **1'** (violet).

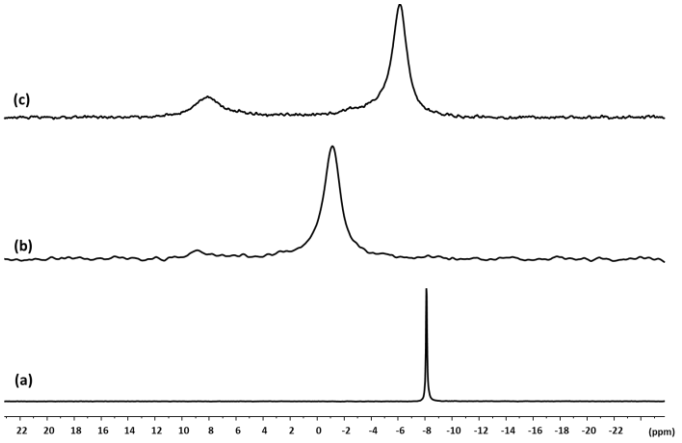

Figure 4. ^{31}P NMR spectra in DMSO-d_6 at 298 K of (a) Me_3PAuCl, (b) complex **1** and (c) complex **1'**.

All attempts to grow single crystals of complex **1** for X-ray analysis were unsuccessful. We thus performed solid-state and 2D liquid NMR analyses to confirm the coordination of the $AuPMe_3$ units on calix[8]arene core and get some structural information. The ^{31}P CP-MAS NMR spectrum of **1** in solid state (Figure S3, Supporting information) displays mostly a single broad signal at –3.6 ppm, deshielded from that of Me_3PAuCl (–9.6 ppm [22]), indicating the coordination of the phosphine groups to the calix[8]arenes, but with some structural or conformational heterogeneity.

Confirmation of the coordination of the Au-PMe_3 groups to the S atoms linked to the calix[8]arene was obtained by using a ^{1}H/^{31}P HETCOR MAS NMR spectroscopy with Frequency-Switched Lee-Goldberg (FSLG) ^{1}H homodecoupling sequence in which the correlation intensity depends on the distance between the phosphorus and proton nuclei. The spectrum registered for complex **1** presents four correlation signals (Figure 5): the first very intense correlation signal at 1.5 ppm corresponds mainly to the phosphine methyl protons and also to the central aliphatic protons of the calix[8]arene alkyl chain; The second correlation at 2.7 ppm corresponds to the protons α to the sulphur atoms, and the third correlation at 4.1 ppm corresponds to the protons α to the oxygen atoms of the alkyl chain of calix[8]arene. The aromatic protons of calix[8]arene, distant from the phosphorus, provide also a weak correlation at 6.6 ppm (Figure 5).

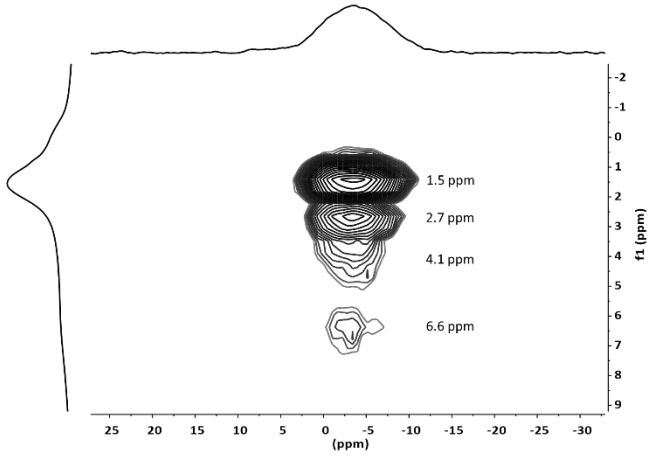

Figure 5. ^{1}H/^{31}P FSLG-HETCOR NMR spectrum (contact time 1 ms) of complex **1** in the solid state.

The analysis of ^{1}H 2D DOSY NMR experiments carried out in DMSO-d_6 (Figure 6) reveals the existence of two diffusion coefficients D for complex **1** equal to $(0.4 \pm 0.1) \times 10^{-10}$ and $(0.8 \pm 0.1) \times 10^{-10}$ m^2 s^{-1}. These diffusion coefficient values are smaller than the value of $(1.1 \pm 0.1) \times 10^{-10}$ m^2 s^{-1} obtained for compound **6** and concern all the protons, even those of the methyl group of PMe_3, thus confirming the coordination of the $AuPMe_3$ groups to the calix[8]arenes. The presence of two D values for complex **1** also indicates the presence of at least two kinds of complexes with different sizes, as the hydrodynamic radius is inversely proportional to the diffusion coefficient. The highest value, corresponding to the main adduct, is slightly smaller than the value obtained for compound **6** indicating that in this case, the eight added AuPME3 groups do not increase so much the size of the complex despite their size. For this complex, the aromatic resonances (Arom-H) are in the range of 6.3 to 6.1 ppm close to value of 6.29 ppm for the compound **6**. This seems to indicate only weak changes of the conformation of the calixarene unit. The slowest diffusing adduct shows aromatic resonances spread between 6.7 to 5.5 ppm evidencing more notable conformational changes. One explanation may lie in the fact that complex **1** may exist as a mixture of different conformations, some of them exhibiting stronger intramolecular aurophilic (Au/Au) or Au-S interactions

between arms (Figure 7). This is consistent with the broadening of the NMR signals, revealing reduced mobilities and/or conformational exchange processes for complex **1** (Figure 3b). However, our results do not allow to determine precisely the conformations of complex **1** in solution. On the other hand, the smallest diffusion coefficient is likely to correspond to a larger species, where the eight "arms" of the calixarene are in their fully expanded conformation. Both species are in slow equilibrium on the NMR timescale.

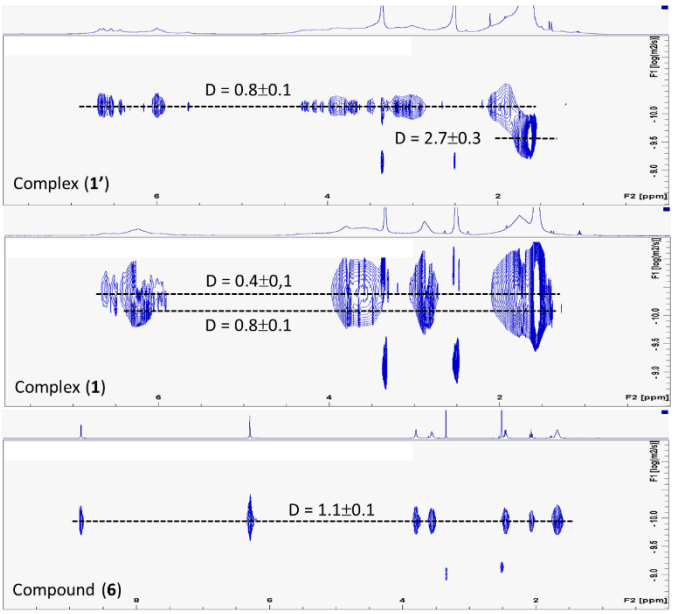

Figure 6. ^{1}H DOSY NMR spectra in DMSO-d_6 at 298K of (Bottom) compound **6**,(middle) complex **1** and (Top) complex **1'**.

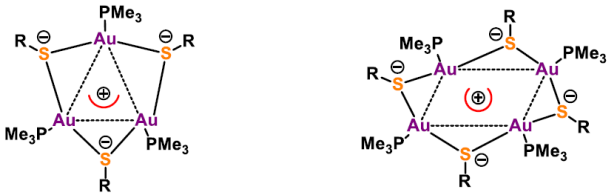

Figure 7. Examples of multinuclear gold complexes formed by aurophilic and multicentered Au-S briges[23]

Increase in gold(I) content. Knowing the tendency of gold thiolates to associate and form multinuclear complexes, the possibility to increase the number of gold atoms per calixarenes was explored. So, complex **1'** was synthesized in situ in an NMR tube, either by addition of eight equivalents of Me_3PAuCl to a DMSO-d_6 solution of complex **1** or by addition of sixteen equivalents of Me_3PAuCl to a DMSO-d_6 solution of calixarene **6**. After addition of eight equivalents of Me_3PAuCl in an NMR tube containing a solution of complex **1** in DMSO-d_6, a global modification of the ^{1}H spectrum is observed (Figure 3c). In particular, the peaks corresponding for the minor adduct of complex **1** show increased intensity of linewidth sharpening. On the other hand, the ones of the major adduct decrease and broaden. Furthermore, only one ^{1}H NMR signal is observed for the PMe_3 protons in complex **1'** at 1.62 ppm, slightly shifted compared to the signal in complex **1** at 1.57 ppm. These result evidence the presence of exchange phenomena for the different adduct complexes and the PMe_3 group. This is strongly confirmed by the ^{31}P NMR spectrum of complex **1'** where only two broad ^{31}P signals are detected at 8.1 ppm and -6.1 ppm, respectively (Figure 4c). No signal of the added Me_3PAuCl precursor is observed. The positions of the signal at 8.1 ppm is similar to the one of complex **1** at 8.9 ppm, but with an important intensity increase. The one at -6.1 ppm is in an intermediate position between the signal of Me_3PAuCl (–8.1 ppm) and the main signal of complex **1** (-1.0 ppm). Taking into account that only one ^{1}H PMe_3 signal is detected, this suggests that the ^{31}P signal at -6.1 ppm is due to a fast exchange between free and complexed PMe_3 groups. ^{31}P-^{31}P EXSY experiment (Figure 8) presents also an exchange correlation between the two P resonances. This indicates that PMe_3 groups of the different adducts are also in intermediate/slow exchange. The ^{31}P signal at 8.1 ppm could then be associated to a more stable adduct that present less symmetry than complex **6** with for example several ^{1}H resonances for aromatic groups (from 6.7 to 5.5 ppm).

As for complex **1**, attempts to grow single crystals suitable for X-ray analysis were unsuccessful, it was also impossible to isolate complex **1'**. So, to get further informations on the possible conformations, 2D liquid NMR experiments were performed. From the ^{1}H 2D DOSY NMR experiments carried out for complex **1'** in DMSO-d_6 (Figure 6), two diffusion coefficients D are determined with values equal to $(0.8 \pm 0.1) \times 10^{-10}$ and $(2.7 \pm 0.3) \times 10^{-10}$ $m^2\ s^{-1}$, respectively. The first value related to the calixarene protons is identical to the highest value obtained for complex **1**, indicating that the global size of complex **1'** is similar and slightly larger than that of compound **6** (with a diffusion coefficient of $(1.1 \pm 0.1) \times 10^{-10}$ $m^2\ s^{-1}$). It also shows that the size of this new complex is comparable to the smallest species observed for **1** (Figure 6). In the same way, we observe the disappearance of the largest specie ($D=0.4 \pm 0.1 \times 10^{-10}$). This shows that the addition of extra $AuPMe_3$ units favors the formation of intramolecular interactions (multinuclear gold complexes and/or aurophilic interactions), resulting in a smaller, compacted structure. The second much higher D value corresponds to the PMe_3 protons and confirms the fast equilibrium between free and complexed PMe_3 groups.

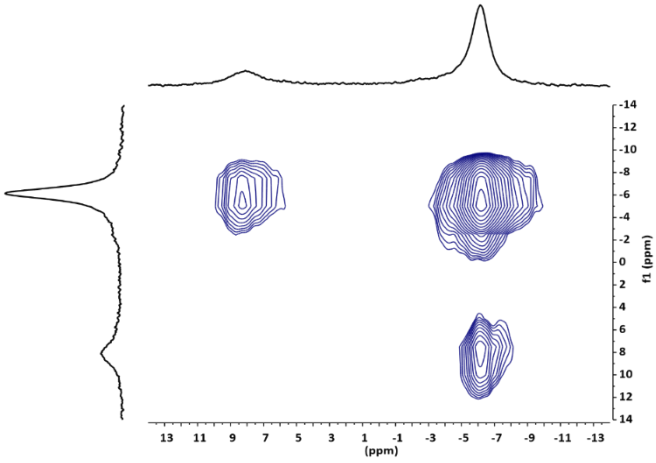

Figure 8. ^{31}P-^{31}P EXSY spectrum of complex **1'** in DMSO-d_6 at 298K.

It is to note that the occurrence of extended intermolecular bridges for **1'** should result in a lowering of the symmetry of the newly formed complexes, that is indeed observed on the corresponding ^{1}H NMR spectrum where the broad resonances previously observed for **1** are replaced by a complex set of well-defined signals (Figure 3). We can thus conclude that a well-defined species is formed (complex **1'**). On the ^{1}H NMR spectrum (Figure 3), eight resonances can be observed for the hydroquinone protons, suggesting for complex **1'** a conformation with a symmetry plane. However, different conformations for complex **1'** do exhibit such a symmetry element (Figure SI), and it is not possible at that point to discriminate between these different possibilities.

Other gold(I)-appended calix[8]arenes

In line with our strategy using benzyloxocalix[8]arenes (compound **2**) as a platform easily functionalised on both rims, other gold-appended calix[8]arenes were prepared following a similar methodology as that reported for complexes **1** and **1'**. As an example, the multi-steps synthesis of compounds **7** and **8** and the corresponding complexes **9** and **10** (Scheme 2) were carried out. These two later complexes were prepared *in situ* in NMR tube by adding 8 equivalents of Me_3PAuCl, in dmso-d_6 solutions of compounds **7** and **8**, respectively. As for complex **1'**, complex **9'** is then obtained by adding 8 more equivalents of Me_3PAuCl in the same NMR tube containing complex **9**. The synthesis and characterizations of these complexes (**9, 10, 9'**) are described in the Supporting Information. These complexes illustrate the fact that the functionalized groups grafted on the calixarenic core can be changed in nature (here by using phosphorylated or benzyloxo groups instead of hydroxyl groups), but also in position on the calixarene (the mercaptobutoxy chains being on the upper rim for complex **9** instead of the lower rim for complexes **1** and **10**).

As previously observed for compound **6** and complex **1**, on-going from compounds **7** and **8** to complexes **9** and **10**, the added gold equivalents have a pronounced influence on the ^{1}H NMR spectra of the corresponding complexes. The addition of 8 equivalents of $ClAuPMe_3$ on compounds **7** and **8** (resulting in complexes **9** and **10**) induces in a strong broadening of the signals (SI figure SA and SB). This is indicative of a reduced conformational flexibility for the resulting complexes, due to the increased size of their substituents, and/or to the occurrence of Au-Au or Au-S intramolecular interactions between the legs of the calixarene (Figure 7). This results in slow conformational interconversion on the NMR timescale.

The addition of 8 more equivalents of Me_3PAuCl to complexes **9** results in the appearance of sharp, well defined signals, indicating that the corresponding complexes **9' e**xist as one (or more) well defined conformation(s). However, it is not possible to precisely determine these conformations. This conformational freezing is attributed to the fact that the extra Me_3PAuCl complexes added to **9** promote the formation of extensive intramolecular bridges between the "legs" of the calixarene, as described for complex **1'**. This bridging effect results in the "locking" of one (or more) calixarenic conformations.

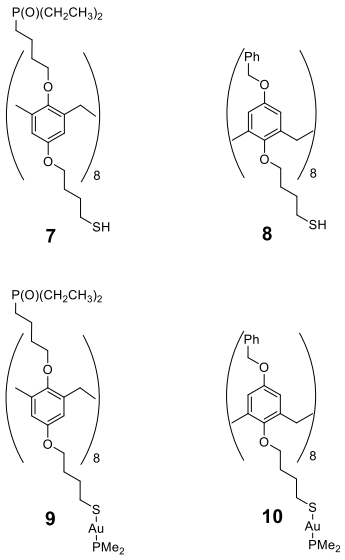

Scheme 2. Compounds **7** and **8**, complexes **9** and **10**.

Synthesis of gold nanoparticles

The previously synthesised complexes **1**, **1'**, **9**, **9'**and **10** were then used to generate Au NPs by reduction under gamma-irradiation. Indeed, radiolysis is a powerful method to generate NPs in solution, since it does not necessitate the addition of any reducing agent, the reducing species (solvated electrons and radicals) being produced *in situ* from the interactions between the ionising radiation and the solvent. So, highly concentrated DMSO solution of the complexes were diluted in ethanol to get a final concentration of 5×10^{-5} mol L^{-1} for complex **1**, **9** and **10**, and 2.5×10^{-5} mol L^{-1} for complex **1'** and **9'**. Then the solutions were bubbled with argon gas to remove dioxygen and then submitted to irradiation till total reduction of Au(I). After irradiation, the solutions are colorless and no localised plasmon resonance band due to Au NPs (expected around 510-520 nm) is observed on the UV-visible spectra. This suggests that the formed NPs are smaller than 5 nm, in accordance with the TEM analysis. Regardless of the complex used, TEM images reveal the formation of small, monodisperse spherical Au NPs with a mean diameter around 2.5 nm for **1** and **1'**, 1.6 nm for **9** and **9'** (Figure 9) and subnanometric in the case of **10** (Figure 10).

It is worth noticing that for the complexes **1** and **1'** (or **9** and **9'**) the size of the observed Au NPs is similar while the amount of Au atoms is doubled. However, as the contrast is quite low and the resolution of our apparatus is not high enough, it is possible that NPs smaller than 1 nm are present but not detected.

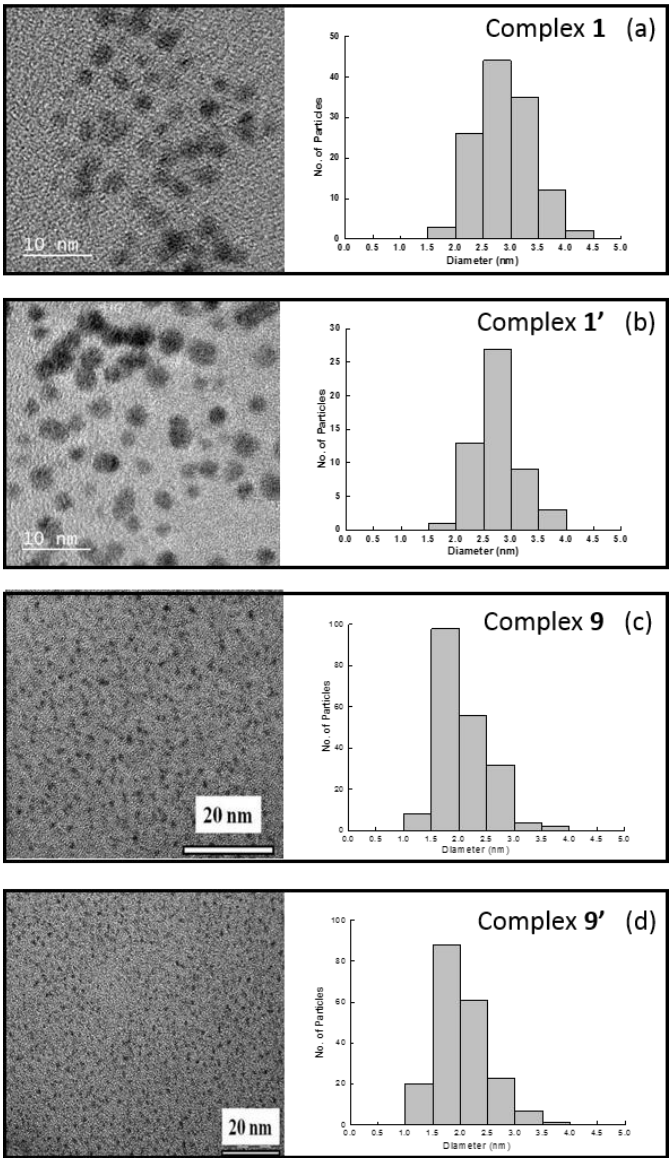

Figure 9. TEM images (left) and size distribution (right) of the gold nanoparticles synthesised by total radiolytic reduction of ethanolic solution containing (a) complex **1**, (b) complex **1'**, (c) complex **9** and (d) complex **9'**

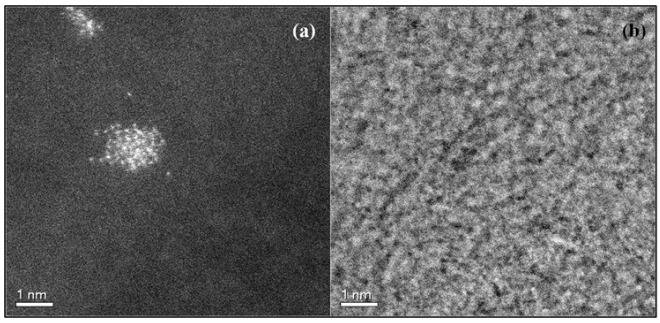

Figure 10. Dark field (a) and bright field (b) TEM images of the gold nanoparticles synthesised by total radiolytic reduction of ethanolic solution containing complex **10**

The nature of the functional group introduced on the calixarene thus seems to exert an influence on the size of the NP, as the presence of phosphate or benzyloxy groups leads to smaller nanoobjects compared to hydroxyl groups. The reason for this effect is not very clear. Possibly, the increased steric protection induced by the bulky benzyloxy or 3-(diethylphosphato)propane groups around the nanoparticules reduces the probability for gold atoms to reach the metallic core of the growing nanoobjects, limiting their growth. A comparison between complexes **1**/**1'** on one hand and **10** on the other hand shows that the (benzyloxy) functionalisation considerably reduces the size of the obtained nanoobjects. This shows that this functionalisation acts as a very efficient passivating layer, considerably slowing the Au atoms flux towards the growing nanoparticles. This may be explained by the fact that these benzyloxy groups do not exert any coordination effect towards Au(I) ions or metallic gold atoms, whereas the phosphate groups do have such a coordination ability. Another explanation may lie in a more compact arrangement of the benzyl groups around the nanoparticle, thus preventing incoming gold atoms to reach the metallic core during the growth.

Conclusion

In this paper, we have presented the synthesis of new gold(I)-appended calix[8]arenes based on a recently developed strategy consisting in using benzyloxycalixarenes as a versatile platform to support metallic complexes. Knowing the affinity of gold to thiolates, we have synthesized calix[8]arenes bearing mercaptobutoxy chain on each ring either on the upper or lower rim. Due to the tendency of gold thiolates to form nuclear complexes, it was possible to append 8 and even 16 Au(I)PMe_3 complexes to each calix[8]arene. Here, octa-Au complexes were successfully isolated by precipitation and filtration. NMR spectroscopy allows to study the dynamics of the formed species. These new complexes can be used as both sources of metal and stabilising agents. Indeed, radiolytic reduction of these complexes leads to the formation of small, monodisperse gold nanoparticles. We have also demonstrated the possibility to directly obtain phosphate-functionalised gold nanoparticles, which could be grafted onto oxide substrates, opening the way to interesting composite nanomaterials and functional surfaces.

Experimental

Materials and synthesis.

All reactions were carried out under argon atmosphere. THF was dried and distilled over sodium/benzophenone, Methanol (MeOH) was distilled over magnesium. Extra dry dimethylformamide (DMF) was purchased from Alfa Aesar. Sodium hydride (NaH) was purchased from Aldrich. All commercially available reagents were used as received.

Synthesis of compounds (**3**, **4**, **5** and **6**) were described previously. [16]

Synthesis of *p*-octa(hydroxyl)-octa[mercaptobutoxy)-gold(I)-trimethylphosphine] calix[8]arene, complex 1: To a degassed solution of **5** (0.150 g, 0.089 mmol, 1 equiv.) in dry THF (17 mL) was

added chloro(trimethylphosphine)gold(I) (0.221 g, 0.715 mmol, 8 equiv.). To the mixture was added dry Et_3N (109 µL, 0.804 mmol, 9 equiv.). The mixture was stirred at rt for 30 min. The mixture was then filtered and the solid washed with THF and was dried under vacuum. The residue was washed under stirring with EtOH (50 mL), then filtered and the residue was dried under vacuum. The product **17** was obtained as a white powder in 52% yield (0.180 g, 0.047 mmol).

^{1}H NMR (400 MHz, DMSO-d_6, ppm): δ 8.77 (s, 8H), 6.25 (m, 16H), 3.81 (s, 16H), 3.61 (m, 16H), 2.87 (m, 16H), 1.77 (m, 32H), 1.55 (m, 52).

^{13}C NMR (400 MHz, DMSO-d_6, ppm): δ 153.22, 148.23, 134.75, 115.41, 73.56, 34.27, 29.82, 15.80.

^{31}P NMR (400 MHz, DMSO-d_6, ppm): δ –1.01 (br s, 1P).

Elemental Analysis: $C_{112}H_{176}Au_8O_{16}P_8S_8$. Theoretical: C 34.86%, H 4.60%, S 6.65%. Measured: C 35.40%, H 4.39%, S 6.87%.

IR (KBr, cm^{-1}): 3198 (*vs*, O-H stretching), 2906 (*s*, C-H stretching), 1595, 1454 (*vs*, aromatic breathing), 1202 (*vs*, C-O stretching), 960 (*vs*, aromatic C-H stretching).

UV-vis spectroscopy (DMSO/EtOH – 20/80) λ_{max} (nm) [ε ($M^{-1}.cm^{-1}$)]: 286 [37000].

XPS (eV): 533.03 (O1s), 284.9 (C1s), 163.19 (S2p), 131.9 (P2p), 84.94 (Au4f).

NMR experiments

1D and 2D ^{1}H, ^{31}P and ^{13}C NMR experiments in liquid state were recorded on either a Bruker DPX 250, Brucker 300 MHz, Bruker Avance 400 or 500 spectrometer. ^{31}P EXSY experiment was acquired with a mixing time of 150 ms.

All diffusion measurements were made using the stimulated echo pulse sequence. The recycle delay was adjusted to 3s. For 2D diffusion ordered spectroscopy (DOSY), after Fourier transformation and baseline correction, the diffusion dimension was processed with the Bruker Topspin software package DOSY (Contin protocole).

Solid-state NMR experiments were recorded on a Bruker AvanceIIIHD 400 spectrometer equipped with a 3.2 mm probe. Samples were spun at 16 kHz at the magic angle using ZrO_2 rotors. ^{31}P-CP/MAS spectra were recorded with a recycle delay of 2 s and contact times of 1 ms. ^{31}P/^{1}H HETCOR experiment was realized with a contact time of 1 ms and with frequency switched Lee-Goldburg homonuclear decoupling during ^{1}H evolution. The ^{1}H-^{31}P FBCP NMR method were performed with a first CP transfer of 2 ms and a second CP contact of 0.05 ms or 2 ms.

All chemical shifts for ^{1}H and ^{13}C are relative to TMS. ^{31}P chemical shifts were referenced to an external 85% H_3PO_4 sample. Data are reported in ppm with the solvent signal as reference.

Instrumentation and analysis

Elemental analyses were performed by the microanalysis service of the Institut de Chimie des Substances Naturelles in Gif-Sur-Yvette(France).

Fourier transform infrared spectra were recorded on a Perkin Elmer Spectrum 100 spectrometer. Organic compounds pellets were prepared using oven dried KBr powder.

X-ray photoelectron measurements were performed on a K alpha (Thermo Fisher) spectrometer equipped with a monochromatic Aluminium source (Al, Ka = 1486.6 eV, beam size: 200 µm).

The gamma irradiations were performed using a ^{60}Co source with a dose rate of 1.8 or 3.7 kGy h^{-1}. The total dose received by the samples was adjusted to totally reduce the gold(I) complexes in ethanolic solution (576 Gy).

Transmission electron microscopy (TEM) images were obtained with a JEOL JEM 100CX or a JEOL1400 operating at 100 and 120 kV, respectively. High angle annular dark field scanning transmission electron microscopy (HAADF-STEM) images were acquired with a JEOL JEM-ARM200F operating at 200 kV. Drops of irradiated solutions were deposited and dried on copper grids coated by amorphous carbon membrane for TEM analysis.

Conflicts of interest

There are no conflicts to declare.

Acknowledgements

The authors thank P. Beaunier (LRS, Sorbonne Université) for TEM analysis and, D. Bahena and M.J. Yacaman (Department of Physics and Astronomy, University of Texas at San Antonio) for HAADF-STEM images. They are also grateful to D. Dragoe (ICMMO, Université Paris-Sud) for XPS measurements. The authors also wish to thanks Charmmmat ANR-11-LABX-0039, grant to I. A.

Notes and references

1 (a) P. Pyykkö, *Angew. Chem. Int. Ed.* 2004, **43**, 4412-4456; (b) D. J. Gorin, F. D. Toste, *Nature*, 2007, **446**, 395-403.

2 (a) A. S. K. Hashmi, *Chem. Rev*. 2007, **107**, 3180-3221; (b) Modern Gold Catalyzed Synthesis, ed. A. S. K. Hashmi, F. D. Toste, Wiley-VCH, Weinheim, Germany, 2012.

3 I. ito, M. Sawamura, T. Hayashi, *J. Am. Chem. Soc.* 1986, **108**, 6405-6406.

4 (a) A. K. Hashmi, G. J. Hutchings, *Angew. Chem. Int. Ed.* 2006, **45**, 7896-7936; (b) N. Marion, S. P. Nolan, *Chem. Soc. Rev.* 2008, **37**, 1776-1782; (c) M. Alcarazo, *Chem. -Eur. J*. 2014, **20**, 1797-1805 ; (d) M. Alcarazo, *Acc. Chem. Res.* 2016, **49**, 1797-1805; (e) B. Ranieri, I. Escofet, A. M. Echavarren, *Org. Biomol, Chem*. 2015, **13**, 7103-7118; (f) A. M. Asiri, A. S. K. Hashmi, *Chem. Soc. Rev*. 2016, **45**, 4471-4503; (g) I. Abdellah, A. Poater, J. F. Lohier, A. C. Gaumont, *Catal. Sci. Tech.* 2018, **8**, 6486-6492.

5 (a) L. T. Ball, G. C. Lloyd-Jones, C. A. Russell, *Science*, 2012, **337**, 1644-1648; (b) L. T. Ball, G. C. Lloyd-Jones, C. A. Russell, *J. Am. Chem. Soc*. 2014, **136**, 254-264.

6 (a) G. Revol, T. McCallum, M. Morin, F. Gagosz, L. Barriault, *Angew. Chem. Int. Ed.* 2013, **52**, 13342-13345; (b) M. S. Winston, W. J. Wolf, F. D. Toste, *J. Am. Chem. Soc.* 2014, **136**, 7777-7782; (c) M. Joost, A. Zeineddine, L. Estévez, S. Mallet-Ladeira, K. Miqueu, A. Amgoune, D. Bourissou, *J. Am. Chem. Soc*. 2014, **136**, 14654-14657; (d) M. Zidan, T. McCallum, L. Thai-Savard, L. Barriault, *Org. Chem. Front*. 2017, **4**, 2092-2096; (e) A. Zieneddine, L. Estévez, S. Mallet-Ladeira, K. Miqueu, A. Amgoune, D. Bourissou, *Nat. Commun*. 2017, **8**, 565.

7 a) P. Gassman, G. Meyer, F. Williams, *J. Am. Chem. Soc*. 1972, **94**, 7741-7748; (b) L. U. Meyer, A. de Meijere, *Tetrahedron Lett*. 1976, **17**, 497-500; (c) C. Y. Wu, T. Horibe, C. B. Jacobsen, F. D. Toste, *Nature*, 2015, **517**, 449-453; (d) M. Joost, L. Estévez, K. Miqueu, A. Amgoune, D. Bourissou*, Angew. Chem. Int. Ed.* 2015, **54**, 5236-5240; (e) F. F. Mulks, S. Faraji, F. Rominger, A. Deruw, A. S. K. Hashmi, *Chem. Eur. J*. 2018, **24**, 71-76.

8 M. Haruta, T. Kobayashi, H. Samo, N. Yamada, *Chem. Lett*. 1987, 405-408.

9 (a) D. Cha, G. Parravano, *J.Catal.* 1970**, 18**, 200-21 ; (b) M. Haruta, M. Daté, *Appl. Catal., A,* 2001**, 222**, 427-437.

10 (a) M. Okumura, T. Akita, M.Haruta, *Catal. Today,* 2002**, 74**, 265 269; (b) P. A. Sermon, G. C. Bond, P. B. Wells, *J. Chem. Soc., FaradayTrans.* 1979**, 75**, 385.

11 N. D. Burrows, W. Lin, J. G. Hinman, J. M. Dennison, A. M. Vartanian, N. S. Abadeer, E. M. Grizincic, L. M. Jacob, J. Li, C. J. Murphy, *Langmuir*, 2016, **32**, 9905-9921.

12 G. J. Hutchings, *ACS Cent. Sci.* 2018, **4**, 1095-1101

13 (a) M. C. Daniel, D. Astruc. *Chem. Rev.* 2004, **104**, 293-346; (b) S. Eustis, M. A. El-Sayed, *Chem. Soc. Rev.* 2006, **35**, 209-217.

14 M. Brust, M. Walker, D. Bethell, D. J. Schiffrin, R. Whyman, *J. Chem. Soc., Chem. Commun*, 1994, 801-802.

15 (a) A. Acharya, K. Samanta, C. Pulla Rao, *Coord. Chem. Rev.* 2012, **256**, 2096-2125; (b) A. R. Kongor, V. A. Mehta, K. M. Modi, M. K. Panchal, S. A. Dey, U. S. Panchal, V. K. Jain, *Top. Curr. Chem*. 2016, **374**, 28.

16 P. Ray, M. Clément, C. Martini, I. Abdellah, P. Beaunier, J. L. Rodriguez-Lopez, V. Huc, H. Remita, I. Lampre*, New. J. Chem.* 2018, **42**, 14128-14137.

17 (a) V. Huc, E. Npetgat, V. Guérineau, S. Bourcier, A. Dos Santos, R. Guillot, J. P. Baltaze, C. Martini*, Eur. J.Org. Chem*. 2010, 6186-6192 ; (b) E. André, B. Boutonnet, P. Charles, C. Martini, J. M. Aguiar-Hualde, S. Latil, V. Guérineau, K. Hammad, P. Ray, R. Guillot, V. Huc, *Eur. Chem. J.* 2016, **22**, 3105-3114. (c) V. Guérineau, M. Rollet, S. Viel, B. Lepoittevin, L. Costa, P. Saint-Aguet, R. Laurent, P. Roger, D. Gigmes, C. Martini, V. Huc, *Nat. Commun*. 2019, **10**, 113.

18 I. Abdellah, P. Kasongo, A. Labattut, R. Guillot, E. Schulz, C. Martini, V. Huc, *Dalton. Trans*. 2018, **47**, 13843-13848.

19 I. Abdellah, C. Martini, A. Dos Santos, D. Dragoe, V. Guérineau, V. Huc, E. Schulz, *ChemCatChem* 2018, **10**, 4761-4767.

20 L. C. Moraes, B. Lacroix, R. C. Figueiredo, P. Lara, J. Rojo, S. Conjero, Dalton. Trans, 2017, **46**, 8367-8371.

21 (a) A. Casnati, R. Ferdani, A. Pochini, R. Ungaro, *J. Org. Chem*. 1997, **62**, 6236-6239 ; (b) P. Leverd, V. Huc, S. Palacin, M. Nierlich, *J. Inclusion Phenom*.*Macrocyclic Chem.* 2000, **36**, 259-266 ; (c) A. Casnati, S. Barboso, H. Rouquette,M.-J. Schwing-Weill, F. Arnaud-Neu, J.-F. Dozol, R. Ungaro, *J. Am. Chem.Soc*. 2001, **123**, 12182-12190; (d) V. Huc, K. Pelzer, *J. Colloid Interface Sci.* 2008, **318**, 1-4.

22 E. N., de Silva, G. A. Bowmaker, P. C. Healy, *J. Mol. Struct*. 2000, **516**, 263-272.

23 A. Sladek, W. Schneider, K. Angermaier, A. Bauer, H. Schmidbaur, *Zeitschrift für Naturforschung B* 1996**, 51**, 765-772.